A Novel Discrete Control Strategy for Independent Stabilization of Parallel Three-Phase Boost Converters by Combining Space-Vector Modulation With Variable-Structure Control

Sudip K. Mazumder, *Member, IEEE*

***Abstract*—We propose a discrete nonlinear controller, developed in a synchronous frame, for a parallel three-phase boost converter consisting of two modules. The basic idea, however, can be extended to a system with N modules. Each of the closed-loop power-converter modules operates asynchronously without any communication with the other modules. The controller stabilizes the currents on the dq-axes and limits the flow of the pure-zero sequence current. It combines the space-vector modulation scheme with a variable-structure control, thereby keeping the switching frequency constant and achieving satisfactory dynamic performance.**

***Index Terms*—Discrete nonlinear controller, N modules, parallel multiphase converters, space-vector modulation, switching frequency, synchronous frame, three-boost converters, variable-structure control.**

I. Introduction

PARALLEL multiphase converters have several advantages, including the capability to handle high power, high reliability, modularity, reconfigurability, less voltage or current ripple, higher efficiency, fast-dynamic response, and lower cost due to reduced cycle time and ease of manufacturing. Therefore, such converters are being increasingly used in applications, such as motor drives, power-factor-correction (PFC) equipments, and uninterruptable power supplies (UPS), distributed power-electronic systems [1]–[5].

Traditionally, a parallel multiphase converter either has a transformer at the ac side [4]–[6] or uses separate power supplies [3]. As such, the converters are not coupled and can be designed individually. This approach, however, results in a bulky and expensive system because of the line-frequency transformer and the additional power supplies.

With the significant improvement in the integrated-power-module technology, it has now become possible and feasible to directly connect three-phase converters in parallel. A three-phase pulse-width modulation (PWM) rectifier, which operates under unity-power-factor condition and regulates the bus voltage, is a viable option for an individual module of such a parallel-converter system. One such system is shown in Fig. 1, which has two modules; it was built in the laboratory [7]–[9], and all of the discussion in this paper is based on this system. We refer to this system as the parallel three-phase boost converter (PTBC), and we refer to the top and the bottom three-phase PWM modules as M1 and M2, respectively. Both M1 and M2 are connected to the same dc distributed bus on the output side and to the three-phase voltage source on the input side.

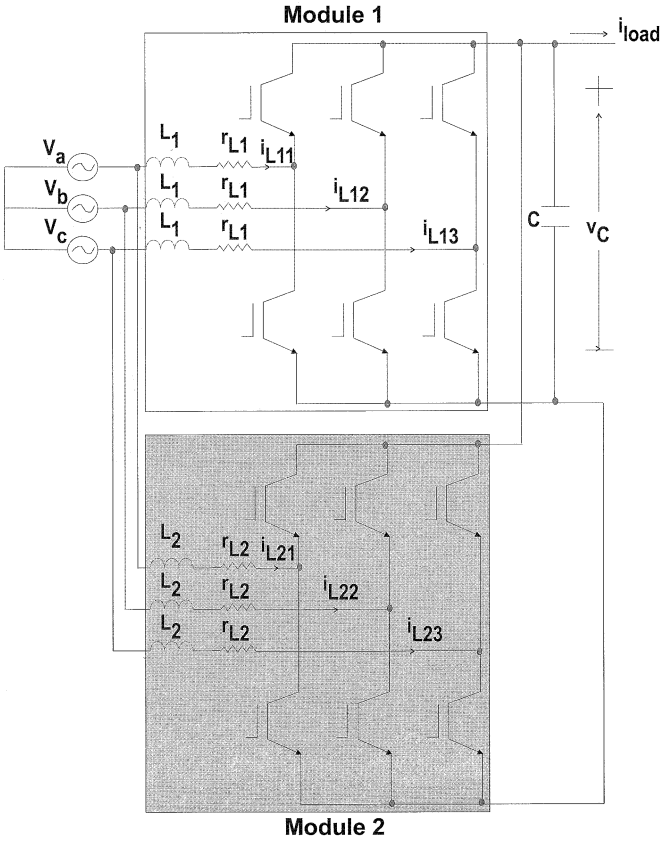

Fig. 1. Schematic of the parallel three-phase boost converter (PTBC).

A. Problem With Parallel Operation of PTBC

When two three-phase PWM modules are directly connected, circulating currents can exist in all of the phases [7], [8], [26], [40]. We illustrate the problem with a simple example. Let us assume that the two modules in Fig. 1 are operating with

Manuscript received February 4, 2002; revised February 5, 2003. Recommended by Associate Editor S. B. Leeb.

The author is with the Power Electronics Research Center, Department of Electrical and Computer Engineering, University of Illinois, Chicago, IL 60616 USA (e-mail: mazumder@ece.uic.edu).

Digital Object Identifier 10.1109/TPEL.2003.813770

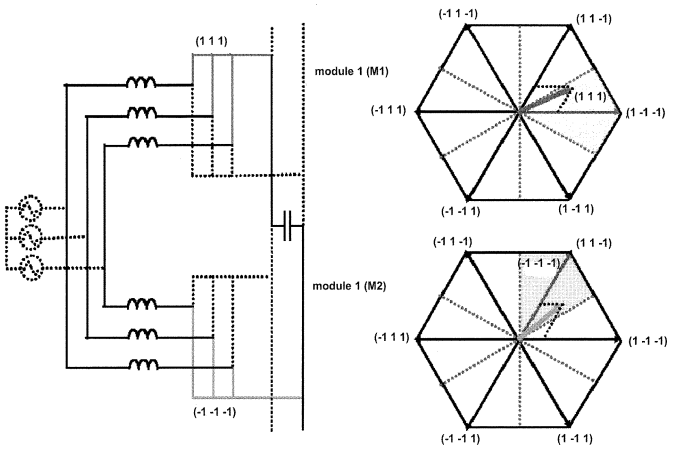

Fig. 2. Slight difference in the position of the reference voltage vectors of the two modules, as shown in the space-vector diagram (right), is responsible for a pure zero-axis current flow. The path of the pure zero-axis current is shown on the left.

bus-clamped space-vector modulation (SVM) [12], [15], [38]. The bus-clamped SVM scheme reduces the switching loss of the PTBC and increase its efficiency. As such, it is one of the most widely used modulation techniques. The hexagonal space-vector representation of the operation of the two modules is shown in Fig. 2 and the operation of the SVM is explained in detail in [36], [38].

For PFC applications, the bus-clamped SVM ensures that the phase carrying the highest current is connected to the bus permanently. This implies that, in Fig. 2, to synthesize the reference voltage vector for module 1, which lies in sector 1 [21], one should use the two active space vectors $(1\ -1\ -1)$ and $(1\ 1\ -1)$ and the zero space vector (1 1 1) in every switching cycle. For module 2 the procedure remains the same [16].

However, in a real world it is impossible to have two modules which are identical. As such, as shown in Fig. 2, at any instant the reference voltage vectors of the two modules may not be at the same location. The reference voltage vector for module two is in sector 2 [21] and is slightly ahead of the reference voltage for module 1. To synthesize it, one should use the zero vector $(-1\ -1\ -1)$ instead of (1 1 1) [7], [8], which is used for module 1. For a standalone three-phase converter, this small change makes no significant difference in stability. However, for the PTBC if at any instant the switching states of the two modules are (1 1 1) and $(-1\ -1\ -1)$, respectively, then a pure zero-axis current is generated [7], [8], [26], [40]. As shown in Fig. 2, the path of this current consist of the bus capacitor and the boost inductors of the two modules. The circulating zero-axis current charges and discharges the three-phase inductors simultaneously. One of the module picks up more current, while the other module drops off a current of the same magnitude. As such, load sharing is lost. Furthermore, because the pure zero-axis current is not reflected on the dq-axes, a dq-axes controller [10], [11] has no effect on the zero-axis current.

B. Existing Solutions and Their Shortcomings

There have been numerous publications regarding the design, operation, and control of three-phase PWM rectifiers [10]–[12]. In a balanced three-phase system, the control is usually implemented in a synchronous reference frame. Such a controller usually controls the currents on the dq axes only because the zero-axis current is negligible for the balanced system. However, when two three-phase PWM modules are directly connected, circulating currents can exist in all of the phases [7], [8]. However, the zero-axis current is not reflected on the dq axes and hence a synchronous-frame controller (in the dq axes) has no effect on the zero-axis current. There are several methods proposed to reduce the cross-current between the modules [1], [2], [13], [14]. Using a linear controller and space-vector modulation (SVM) schemes, which do not use the zero vectors, Xing *et al.* [7], [8] have developed schemes for standardized three-phase modules to reduce the cross-current. The advantage of such schemes is that the communication between the modules is minimal. However, the transient response of the PTBC is not satisfactory and the magnitude of the zero-sequence current under steady-state conditions is not shown. Korondi *et al.* [37] have developed a controller for a three-phase standalone inverter, which is capable of operating with an unbalanced load. The controller operates in the $\alpha\beta$ frame. To ensure sinusoidal output waves, the $\alpha\beta$ components are controlled nonideally using a hysteresis relay with an additional zero-phase-sequence elimination. Ye *et al.* [26] have put forward a similar idea to control a PTBC instead of a standalone converter. In this paper, we will refer to this control scheme as CS_{Ye}. The linear control scheme is simple and minimizes the zero-sequence current under steady-state condition by simply varying the duration of the zero space vector. However, if the system saturates, the control scheme will not work effectively, even under steady-state conditions. This is because, when the system saturates, the zero vector cannot be applied [39]. Furthermore, the performance of the system under dynamic conditions has not been demonstrated [26]. Finally, the implementation of this scheme requires that the duration of the zero vectors of one of the modules of the PTBC is fixed [26].

II. New Proposition

In this paper, we extend the work in [7], [8], [26] using a discrete nonlinear controller (VSC). A closed-loop PTBC is a nonlinear, nonminimum phase system. Hence, the stability of the closed-loop system using the control schemes described in [26] may not be guaranteed except in the vicinity of a periodic orbit. By using a nonlinear controller, we intend to improve the stability and the dynamic performance of the PTBC under varying operating conditions. The proposed scheme combines SVM with a variable-structure controller (VSC). We believe, this is the first time that such a control scheme has been developed to control a PTBC. Using this scheme, we can keep the frequency of the power-converter modules constant under steady state and retain the superior dynamic performance of VSC [17], [18] even when the two modules switch asynchronously and have different switching frequencies. Hence, clock synchronization of the two modules is not necessary [7]–[9].

III. Modeling and Analysis of the Parallel Three-Phase Boost Converter

In Fig. 1, we show a schematic of a PTBC with two power modules. For each individual module, we assume that the varia-

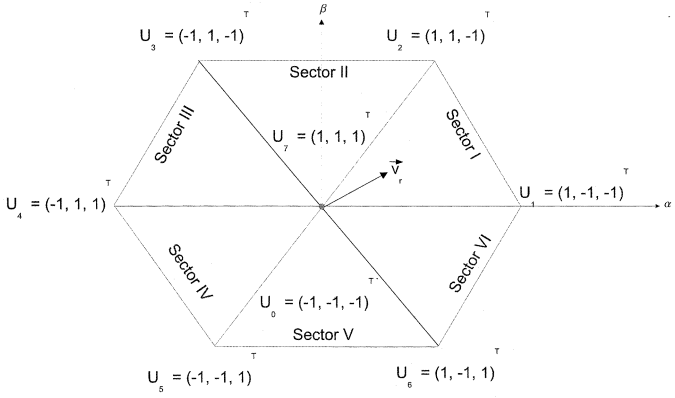

Fig. 3. Distribution of the space vectors in the $\alpha\beta$ frame.

tion in the line inductance of each phase is negligible. However, the line inductances for two different modules are different. We also assume that the esr of the output capacitor is negligible and the input voltages are balanced; that is, $V_a + V_b + V_c = 0$.

Based on Fig. 1, we obtain the following differential equations (with discontinuous right-hand sides) that describe the dynamics of the PTBC

$$\dot{v}_C(t) = -\frac{1}{C} i_{load}(t) + \frac{1}{2C}\sum_{k=1}^{2}\left(\sum_{j=1}^{3} i_{L_{kj}}(t) u_{kj}(t)\right)$$

$$\begin{aligned}\dot{\vec{i}}_{L_k}^{abc}(t) &= (P_{k1}+P_{k2})\vec{i}_{L_k}^{abc}(t) + P_{k3}\vec{V}_{abc}(t) \\ &\quad + P_{k4}\vec{u}_1^{abc}(t)v_C(t) + P_{k5}\vec{u}_2^{abc}(t)v_C(t). \end{aligned} \tag{1}$$

In (1) and for the rest of the paper, $k = 1$ and 2. The vectors representing the phase currents and switching functions of M1 and M2 are given by

$$\vec{i}_{L_k}^{abc}(t) = [i_{L_{k1}}(t)\ i_{L_{k2}}(t)\ i_{L_{k3}}(t)]^T \tag{2}$$

and

$$\vec{u}_k^{abc}(t) = [u_{k1}(t)\ u_{k2}(t)\ u_{k3}(t)]^T \tag{3}$$

respectively. In (1), $\vec{V}_{abc} = [V_a\ V_b\ V_c]^T$ and the matrices $P_{ki}(i = 1, 2, \cdots 5)$ are given in Appendix I. For the PTBC, the top and bottom switches of any phase are complementary in nature. The switching functions $u_{kj}(j = 1, 2, 3)$ attain a value of -1 (or 1) if the bottom (or top) switch of any phase is on. For the boost converter, $\vec{u}_1^{abc}(t)(\vec{u}_2^{abc}(t))$ can attain only eight discrete values ($U_0 = [-1\ -1\ -1]^T$, $U_1 = [1\ -1\ -1]^T$, $U_2 = [1\ 1\ -1]^T$, $U_3 = [-1\ 1\ -1]^T$, $U_4 = [-1\ 1\ 1]^T$, $U_5 = [-1\ -1\ 1]^T$, $U_6 = [1\ -1\ 1]^T$, $U_7 = [1\ 1\ 1]^T$) for feasible operation, as shown in Fig. 3. Two of these (U_0 and U_7) are the zero vectors, while the other six are the active vectors. For convenience, we will drop the notation of time from now on.

If we define the zero-sequence component of the two modules as

$$i_{L_{ko}} = \frac{1}{3}\sum_{j=1}^{3} i_{L_{kj}} \tag{4}$$

then we rewrite (1) as

$$\dot{\vec{i}}_{L_k}^{abc} - P_{ko}\dot{i}_{L_{ko}} = -\frac{r_{Lk}}{L_k}\left(\vec{i}_{L_k}^{abc} - P_{ko}i_{L_{ko}}\right) + P_{k3}\vec{V}_{abc} - P_{k3}\vec{u}_k^{abc}v_C \tag{5}$$

where $P_{ko} = [1\ 1\ 1]^T$. Equation (5) shows that, if the zero-sequence currents of M1 and M2 are zero, then the PTBC behaves as two independent three-phase boost converters. However, for all practical purposes, the two modules will not be identical, and hence $i_{L_{1o}}$ and $i_{L_{2o}}$ are not equal to zero. However, based on Fig. 1 and Kirchoff's current law, the zero-axis currents must satisfy the constraint

$$\sum_k i_{L_{ko}} = 0. \tag{6}$$

Next, we consider the generic transformation

$$\vec{\chi}^{abc} = [T(\theta)]^{-1}\vec{\chi}^{dqo} \tag{7}$$

where $\vec{\chi}^{dqo} = [\chi_d\ \chi_q\ \chi_o]^T$ and $[T(\theta)]^{-1}$ is a nonsingular matrix (given in Appendix II). The components χ_d, χ_q, and χ_o are referred to as the active, reactive, and the zero-axis components of $\vec{\chi}^{dqo}$. Using (7) and

$$\theta = \theta(t_0) + \int_0^t \omega d\tau \tag{8}$$

where ω is the line frequency, we rewrite (1) as

$$\begin{aligned}\dot{v}_C &= -\frac{1}{C} i_{load} + \frac{1}{C}\left(i_{L_{kd}}u_{kd} + i_{L_{kq}}u_{kq} + i_{L_{ko}}u_{ko}\right) \\ \dot{\vec{i}}_{L_k}^{dqo} &= T(\theta)(P_{k1}+P_{k2})[T(\theta)]^{-1}\vec{i}_{L_k}^{dqo} + T(\theta)P_{k3}[T(\theta)]^{-1}\vec{V}^{dqo} \\ &\quad + T(\theta)P_{k4}[T(\theta)]^{-1}\vec{u}_1^{dqo}v_C + T(\theta)P_{k5}[T(\theta)]^{-1}\vec{u}_2^{dqo}v_C \\ &\quad - T(\theta)\frac{d}{d\theta}[T(\theta)]^{-1}\vec{i}_{L_k}^{dqo}. \end{aligned} \tag{9}$$

In (9)

$$\begin{aligned}\vec{i}_{L_k}^{dqo} &= \left[i_{L_{kd}}\ i_{L_{kq}}\ i_{L_{ko}}\right]^T \\ \vec{V}^{dqo} &= [V_d\ V_q\ V_o]^T \\ \vec{u}_k^{dqo} &= [u_{kd}\ u_{kq}\ u_{ko}]^T \end{aligned} \tag{10}$$

where $V_q = V_o = 0$ because we have assumed that the line voltages are balanced.

Using Appendices I and II, we simplify (9) to

$$\dot{v}_C = -\frac{1}{C} i_{load} + \frac{1}{2C}\sum_{k=1}^{2}\left(i_{L_{kd}}u_{kd} + i_{L_{kq}}u_{kq} + i_{L_{ko}}u_{ko}\right)$$

$$\begin{aligned}\dot{\vec{i}}_{L_1}^{dqo} = \begin{bmatrix}\dot{i}_{L_{1d}}\\ \dot{i}_{L_{1q}}\\ \dot{i}_{L_{1o}}\end{bmatrix} &= \begin{bmatrix}-\frac{r_{L1}}{L_1} & \omega & 0\\ -\omega & -\frac{r_{L1}}{L_1} & 0\\ 0 & 0 & -\frac{r_{L1}+r_{L2}}{L_1+L_2}\end{bmatrix} \\ &\quad \times \begin{bmatrix}i_{L_{1d}}\\ i_{L_{1q}}\\ i_{L_{1o}}\end{bmatrix} + \frac{1}{L_1}\begin{bmatrix}V_d\\ V_q\\ V_o\end{bmatrix} \\ &\quad - \frac{v_C}{2L_1}\begin{bmatrix}1 & 0 & 0\\ 0 & 1 & 0\\ 0 & 0 & \frac{L_1}{L_1+L_2}\end{bmatrix} \\ &\quad \times \begin{bmatrix}u_{1d}\\ u_{1q}\\ u_{1o}\end{bmatrix} - \frac{v_C}{2L_1}\begin{bmatrix}0\\ 0\\ -\frac{L_1}{L_1+L_2}u_{2o}\end{bmatrix} \end{aligned}$$

$$\dot{\vec{i}}_{L_2}^{dqo} = \begin{bmatrix}\dot{i}_{L_{2d}}\\ \dot{i}_{L_{2q}}\\ \dot{i}_{L_{2o}}\end{bmatrix} = \begin{bmatrix}-\frac{r_{L2}}{L_2} & \omega & 0\\ -\omega & -\frac{r_{L2}}{L_2} & 0\\ 0 & 0 & -\frac{r_{L1}+r_{L1}}{L_1+L_2}\end{bmatrix}$$

$$\times \begin{bmatrix} i_{L_{2d}} \\ i_{L_{2q}} \\ i_{L_{2o}} \end{bmatrix} + \frac{1}{L_2} \begin{bmatrix} V_d \\ V_q \\ V_o \end{bmatrix}$$
$$\times -\frac{v_C}{2L_2} \begin{bmatrix} 1 & 0 & 0 \\ 0 & 1 & 0 \\ 0 & 0 & \frac{L_2}{L_1+L_2} \end{bmatrix}$$
$$\times \begin{bmatrix} u_{2d} \\ u_{2q} \\ u_{2o} \end{bmatrix} - \frac{v_C}{2L_2} \begin{bmatrix} 0 \\ 0 \\ -\frac{L_2}{L_1+L_2} u_{1o} \end{bmatrix}. \quad (11)$$

Equation (11) shows that, for each module, the dynamical equations governing the currents on the dq axes depend only on $u_{1d}(u_{2d})$ and $u_{1q}(u_{2q})$. The differential equations describing the zero-axis currents (for both the modules) involve a cross-coupling control term. However, if we treat $u_{2o}(u_{1o})$ as a disturbance for $\dot{i}_{1o}(\dot{i}_{2o})$, then the dynamics of the three currents are governed by three fictitious but independent controls on the dqo axes.

We note that $\dot{i}_{L_{1d}}(\dot{i}_{L_{2d}})$ and $\dot{i}_{L_{1q}}(\dot{i}_{L_{2q}})$ are not affected by $i_{L_{1o}}(i_{L_{2o}})$. If $u_1^{abc} = U_7$ and $u_2^{abc} = U_0$ or vice-versa, then using (7), (11), and

$$\cos(\theta) + \cos\left(\theta - \frac{2\pi}{3}\right) + \cos\left(\theta - \frac{4\pi}{3}\right) = 0,$$
$$\sin(\theta) + \sin\left(\theta - \frac{2\pi}{3}\right) + \sin\left(\theta - \frac{4\pi}{3}\right) = 0 \quad (12)$$

we can show that a pure zero-sequence current flows from one module to the other and $u_{1d}(u_{2d})$ and $u_{1q}(u_{2q})$ are equal to zero. During this time, the utility is isolated from the bus. For all other switching configurations, the zero-sequence current exists but $u_{1d}(u_{2d})$ and $u_{1q}(u_{2q})$ are not equal to zero.

IV. Discrete Controller

A. Objectives and Architecture

The objectives of the control are three fold. First, the bus voltage should be regulated at 400 volts. Second, the phase currents of each module should be synchronous with the input phase voltages. Third, the two modules should share the power consumed by the load equally. However, these objectives have to be met by controlling the two modules as independently as possible.

The architecture of the controller is shown in Fig. 4. The controllers for the two modules have a multiloop structure, with an outer voltage loop and an inner current loop. The only common feedback to both modules is the d-axis reference current $(i^*_{L_{kd}})$ obtained from the outer voltage loop, which serves as the master. We use a common voltage loop because both modules are connected over a common dc bus. The reference currents for the q-axis $(i^*_{L_{kq}})$ and the o-axis $(i^*_{L_{ko}})$ are maintained equal to zero to achieve unity-power-factor operation and minimize the zero-axis interaction between the two modules. The current loops are designed to be fast so that the closed-loop system can reject the feedforward and feedback disturbances and regulate the output voltage. The outer voltage loop is designed to be slow and is based on a linear lag-lead controller with an integrator [7], [8], [11], [15].

Mazumder [40] showed that it is impossible to control all of the six currents in (2) independently. Therefore, we define the

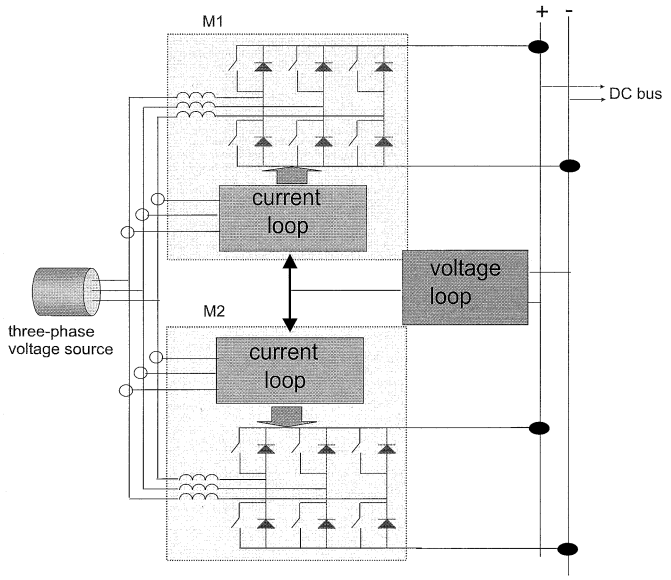

Fig. 4. Block diagram of the closed-loop PTBC.

following five sliding surfaces [17]–[19] to attain the control objectives

$$\sigma_{kd} = i^*_{L_{kd}} - i_{L_{kd}} = 0$$
$$\sigma_{kq} = i^*_{L_{kq}} - i_{L_{kq}} = 0$$
$$\sigma_{1o} = i^*_{L_{1o}} - i_{L_{1o}} = 0 \quad (13)$$

where $k = 1, 2$. While independent control of σ_{kd} and σ_{kq} is possible, it is impossible to control σ_{1o} independently without any communication between the two modules [40]. However, controlling the manifold

$$(\sigma_{1d}=0)\bigcap(\sigma_{1q}=0)\bigcap(\sigma_{1o}=0)\bigcap(\sigma_{2d}=0)\bigcap(\sigma_{2q}=0) \quad (14)$$

is still possible using one or more of the following alternatives: increasing the values of the line inductances, increasing the switching frequencies of the modules, eliminating the use of zero-space vectors [7], [8], or constraining $||u_{1o} - u_{2o}||$ on a reduced-order manifold [40]. The first alternative makes the size of the PTBC larger and the second one increases the switching losses and stresses of the power devices significantly. The last two options do not require an increase in the boost inductance or the switching frequency to minimize σ_{1o}. Although using the third option we can minimize the zero-sequence current [7], the magnitude of the zero-sequence current is higher than achieved using the last option [40]. Furthermore, implementation of option three increases the switching ripple of the current [7], [40]. Therefore, we choose the third option.

B. Scheme

We look for stability on a reduced-order manifold, where instead of controlling $u_{1o} - u_{2o}$ (or $u_{2o} - u_{1o}$), we control their averages; that is, $\overline{u}_{1o} - \overline{u}_{2o}(\overline{u}_{2o} - \overline{u}_{1o})$. An additional problem that we found in [40] is related to the switching frequency. Sliding-mode control tries to optimize the magnitude of switching [17], [19], and hence it cannot guarantee that the switching frequency is constant. However, using hysteresis (as

in our analog schemes), the switching frequency can be kept reasonably constant under steady state [20]. On other hand, the control of three-phase boost converters using space-vector modulation (SVM) schemes [21]–[25] ensures a fixed switching frequency. However, the stability of these controllers, developed based on small-signal analysis, cannot be guaranteed except in the vicinity of the equilibrium solution.

In this section, we develop a discrete control scheme for the current-loop of the PTBC. The objective of the current loop is to stabilize the PTBC on the dq axes and keep the zero-axis disturbance bounded. The outer loop of the overall control system that regulates the bus voltage is designed using a linear controller such that the impact of the higher-order line frequencies on the closed-loop system is minimized.

An important feature of the discrete control scheme is that it keeps the switching frequency constant by combining VSC with SVM techniques. The control scheme can be combined with any SVM scheme. However, not all of the SVM techniques can be used to reject the disturbance due to the zero-axis currents [8]. Therefore, we chose the SVM scheme outlined in [7], [8], [26] to control the zero-axis current. In any given switching cycle, this SVM scheme synthesizes a reference voltage vector ($\vec{v}_r$) (see Fig. 3) using two zero vectors and two active vectors. For example, if $\vec{v}_r$ is in Sector I, then it is synthesized as [21]–[25]

$$\vec{v}_r = \frac{v_C}{2T}(t_1U_0 + t_2U_1 + t_3U_2 + t_4U_7 + t_5U_2 + t_6U_1 + t_7U_0) \tag{15}$$

where $T = t_1 + t_2 + t_3 + t_4 + t_5 + t_6 + t_7$.

Having selected the SVM scheme, we need to express $i_{L_{kd}}$ and $i_{L_{kq}}$ in discrete form to implement the current loop using the DVSC. The discrete form of $\vec{i}_{L_k}^{dq}$ is a map of the form

$$\vec{i}_{L_k}^{dq}(n+1) = F_k\left(\vec{i}_{L_k}^{dq}(n), \vec{V}^{dq}(n), \vec{t}_k^{dq}(n)\right) \tag{16}$$

where $\vec{i}_{L_k}^{dq} = [i_{L_{kd}}\ i_{L_{kq}}]^T$, $\vec{V}^{dq} = [V_d\ V_q]^T$, and $\vec{t}_k^{dq} = [t_{kd}\ t_{kq}]^T$. To obtain the map (16), we first solve for $\vec{i}_{L_k}^{dq}$ (using (11)) in each time interval of the space-vector modulated waveform. One such waveform is shown in Fig. 5, which is valid only for Sector I. We start by solving for $i_{L_{kd}}$ and $i_{L_{kq}}$ in Sector I for each interval of time. Once we obtain all of the solutions, we obtain a map that relates $i_{L_{kd}}$ and $i_{L_{kq}}$ at the end of a switching cycle with those at the beginning. Subsequently, using this map, which is valid only for Sector I, we obtain the generalized map (16).

Fig. 5 shows that, although there are seven intervals of time in a given switching cycle, only three of them are distinct. Using (11), (12), and noting that (7) relates $\vec{u}_k^{dq}$ to $\vec{u}_k^{abc}$, we rewrite the dynamical equations for $i_{L_{kd}}$ and $i_{L_{kq}}$ in each of these distinct intervals of time as

{time interval a-b, d-e, and g-h}

$$\dot{\vec{i}}_{L_k}^{dq} = \begin{bmatrix} \dot{i}_{L_{kd}} \\ \dot{i}_{L_{kq}} \end{bmatrix} = \begin{bmatrix} -\frac{r_{L_k}}{L_k} & \omega \\ -\omega & -\frac{r_{L_k}}{L_k} \end{bmatrix} \begin{bmatrix} i_{L_{kd}} \\ i_{L_{kq}} \end{bmatrix} + \frac{1}{L_k}\begin{bmatrix} V_d \\ V_q \end{bmatrix} = A_k\vec{i}_{L_k}^{dq} + B_k\vec{V}^{dq} \tag{17}$$

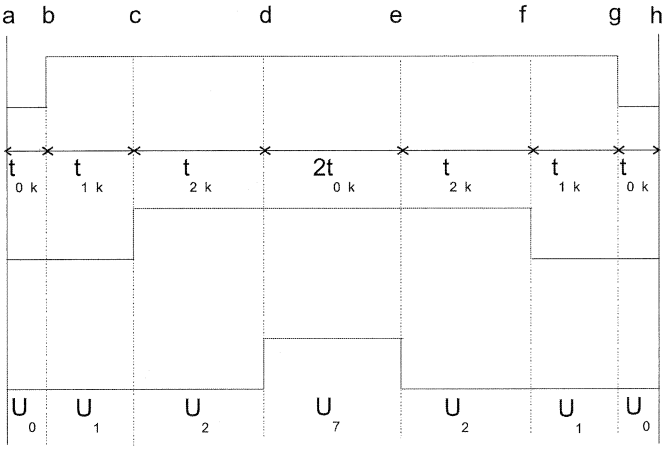

Fig. 5. Sample space-vector modulated waveform to synthesize the reference voltage vector in Sector I.

{time interval b-c and f-g}

$$\begin{aligned}\dot{\vec{i}}_{L_k}^{dq} = \begin{bmatrix} \dot{i}_{L_{kd}} \\ \dot{i}_{L_{kq}} \end{bmatrix} &= \begin{bmatrix} -\frac{r_{L_k}}{L_k} & \omega \\ -\omega & -\frac{r_{L_k}}{L_k} \end{bmatrix} \begin{bmatrix} i_{L_{kd}} \\ i_{L_{kq}} \end{bmatrix} + \frac{1}{L_k}\begin{bmatrix} V_d \\ V_q \end{bmatrix} \\ &\quad - \frac{v_C}{2L_k}\begin{bmatrix} \frac{4}{3} \\ 0 \end{bmatrix}\cos(\theta) - \frac{v_C}{2L_k}\begin{bmatrix} 0 \\ -\frac{4}{3} \end{bmatrix}\sin(\theta) \\ &= A_k\vec{i}_{L_k}^{dq} + B_k\vec{V}^{dq} + v_C C_{k1}\cos(\theta) \\ &\quad + v_C C_{k2}\sin(\theta)\end{aligned} \tag{18}$$

{time interval c-d and e-f}

$$\begin{aligned}\dot{\vec{i}}_{L_k}^{dq} = \begin{bmatrix} \dot{i}_{L_{kd}} \\ \dot{i}_{L_{kq}} \end{bmatrix} &= \begin{bmatrix} -\frac{r_{L_k}}{L_k} & \omega \\ -\omega & -\frac{r_{L_k}}{L_k} \end{bmatrix} \begin{bmatrix} i_{L_{kd}} \\ i_{L_{kq}} \end{bmatrix} + \frac{1}{L_k}\begin{bmatrix} V_d \\ V_q \end{bmatrix} \\ &\quad - \frac{v_C}{2L_k}\begin{bmatrix} \frac{2}{3} \\ \frac{2}{\sqrt{3}} \end{bmatrix}\cos(\theta) - \frac{v_C}{2L_k}\begin{bmatrix} \frac{2}{\sqrt{3}} \\ -\frac{2}{3} \end{bmatrix}\sin(\theta) \\ &= A_k\vec{i}_{L_k}^{dq} + B_k\vec{V}^{dq} + v_C D_{k1}\cos(\theta) \\ &\quad + v_C D_{k2}\sin(\theta).\end{aligned} \tag{19}$$

The closed-form solution of (17) is [27]–[30]

$$\begin{aligned}\vec{i}_{L_k}^{dq}(m+1) &= e^{A_k t_{0k}}\vec{i}_{L_k}^{dq}(m) + (e^{A_k t_{0k}} - I)A_k^{-1}B_k\vec{V}^{dq} \\ &= \Phi_{k1}\vec{i}_{L_k}^{dq}(m) + \Gamma_{k1}\vec{V}^{dq} + \Omega_{k1}v_C(n)\end{aligned} \tag{20}$$

where m represents the m^{th} sub-sampling period in the n^{th} sampling period, $\vec{i}_{L_k}^{dq}(m)$ is the initial value of $\vec{i}_{L_k}^{dq}$ at the beginning of the sub-interval, and t_0 is the duration of the sub-interval. A closed-form solution of (18) is not possible. To proceed further, we assume that the bus voltage is constant through out a sampling interval. Then the solution of (18) is given by

$$\begin{aligned}\vec{i}_{L_k}^{dq}(m+1) &= e^{A_k t_{1k}}\vec{i}_{L_k}^{dq}(m) + (e^{A_k t_{1k}} - I)A_k^{-1}B\vec{V}^{dq} \\ &\quad + v_C(n)\int_{t_k(m)}^{t_k(m)+t_{1k}} e^{A_k(t_k(m)+t_{1k}-\xi)} \\ &\quad \times C_{k1}\cos(\omega\xi)d\xi \\ &\quad + v_C(n)\int_{t_k(m)}^{t_k(m)+t_{1k}} e^{A_k(t_k(m)+t_{1k}-\xi)} \\ &\quad \times C_{k2}\sin(\omega\xi)d\xi.\end{aligned} \tag{21}$$

To obtain the closed-form solution of (21), we let

$$\psi = t_k(m) + t_{1k} - \xi \tag{22}$$

which implies that

$$\begin{aligned} d\psi &= -d\xi \\ \xi &= t_k(m) + t_{1k} - \psi. \end{aligned} \tag{23}$$

Using (22) and (23), we rewrite (21) using hyperbolic functions as

$$\begin{aligned} \vec{i}_{L_k}^{dq}(m+1) &= e^{A_k t_{1k}} \vec{i}_{L_k}^{dq}(m) + (e^{A_k t_{1k}} - I) A_k^{-1} B_k \vec{V}^{dq} \\ &+ v_C(n) \int_0^{t_{1k}} e^{A_k \psi} C_{k1} \\ &\times \left(\frac{e^{i\omega(t_k(m)+t_{1k}-\psi)} + e^{-i\omega(t_k(m)+t_{1k}-\psi)}}{2} \right) d\psi \\ &+ v_C(n) \int_0^{t_{1k}} e^{A_k \psi} C_{k2} \\ &\times \left(\frac{e^{i\omega(t_k(m)+t_{1k}-\psi)} - e^{-i\omega(t_k(m)+t_{1k}-\psi)}}{2i} \right) d\psi. \end{aligned} \tag{24}$$

Now, the eigenvalues of $A_k (= -(r_{L_k}/L_k) \pm i\omega)$ are distinct, and hence we can write $e^{A_k \psi}$ as

$$e^{A_k \psi} = M_k e^{\Lambda_k \psi} M_k^{-1} \tag{25}$$

where M_k is the modal matrix whose columns are the eigenvectors of A_k. The matrix Λ_k is diagonal and its elements are the eigenvalues of A_k. As such, $e^{\Lambda_k \psi}$ is also a diagonal matrix. Using (25), we rewrite (24) as

$$\begin{aligned} \vec{i}_{L_k}^{dq}(m+1) &= e^{A_k t_{1k}} \vec{i}_{L_k}^{dq}(m) + \left(e^{A_k t_{1k}} - I\right) A_k^{-1} B_k \vec{V}^{dq} \\ &+ v_C(n) e^{i\omega(t_k(m)+t_{1k})} M_k \int_0^{t_{1k}} \\ &\times \left(\frac{e^{(\Lambda_k - i\omega I)\psi} + e^{(\Lambda_k + i\omega I)\psi}}{2} \right) \\ &\times M_k^{-1} C_{k1} d\psi + v_C(n) e^{i\omega(t_k(m)+t_{1k})} M_k \int_0^{t_{1k}} \\ &\times \left(\frac{e^{(\Lambda_k - i\omega I)\psi} - e^{(\Lambda_k + i\omega I)\psi}}{2i} \right) \\ &\times M_k^{-1} C_{k2} d\psi \end{aligned} \tag{26}$$

where I is the identity matrix having the same dimension as A_k. Finally, we obtain the closed-form solution of (26) as

$$\begin{aligned} \vec{i}_{L_k}^{dq}(m+1) &= e^{A_k t_{1k}} \vec{i}_{L_k}^{dq}(m) + (e^{A_k t_{1k}} - I) A_k^{-1} B \vec{V}^{dq} \\ &+ v_C(n) \left(\frac{e^{i\omega(t_k(m)+t_{1k})}}{2} M_k \left(e^{(\Lambda_k - i\omega I) t_{1k}} - I \right) \right. \\ &\times (\Lambda_k - i\omega I)^{-1} M_k^{-1} C_{k1} \\ &+ \frac{e^{-i\omega(t_k(m)+t_{1k})}}{2} M_k \left(e^{(\Lambda_k + i\omega I) t_{1k}} - I \right) \\ &\times (\Lambda_k + i\omega I)^{-1} M^{-1} C_{k1} \Big) \\ &+ v_C(n) \left(\frac{e^{i\omega(t_k(m)+t_{1k})}}{2i} M_k \left(e^{(\Lambda_k - i\omega I) t_{1k}} - I \right) \right. \\ &\times (\Lambda_k - i\omega I)^{-1} M_k^{-1} C_{k2} \\ &- \frac{e^{-i\omega(t_k(m)+t_{1k})}}{2i} M_k \left(e^{(\Lambda_k + i\omega I) t_{1k}} - I \right) \\ &\times (\Lambda_k + i\omega I)^{-1} M_k^{-1} C_{k2} \Big). \end{aligned} \tag{27}$$

The solution of (19) can be found directly from (27) by replacing C_{k1} with D_{k1} and C_{k2} with D_{k2}. If the switching frequency of the PTBC is high, then we can assume that during one switching cycle θ is constant. Therefore, (27) simplifies to

$$\begin{aligned} \vec{i}_{L_k}^{dq}(m+1) &= e^{A_k t_{1k}} \vec{i}_{L_k}^{dq}(m) + (e^{A_k t_{1k}} - I) A_k^{-1} B \vec{V}^{dq} \\ &+ \left((e^{A_k t_{1k}} - I) A_k^{-1} C_{k1} \cos(\theta(n)) \right. \\ &+ \left. (e^{A_k t_{1k}} - I) A_k^{-1} C_{k2} \sin(\theta(n)) \right) v_C(n) \\ &= \Phi_{k2} \vec{i}_{L_k}^{dq}(m) + \Gamma_{k2} \vec{V}^{dq} + \Omega_{k2} v_C(n). \end{aligned} \tag{28}$$

Then, using (28), we obtain the solution of (19) as

$$\begin{aligned} \vec{i}_{L_k}^{dq}(m+1) &= e^{A_k t_{2k}} \vec{i}_{L_k}^{dq}(m) + (e^{A_k t_{2k}} - I) A_k^{-1} B_k \vec{V}^{dq} \\ &+ \left((e^{A_k t_{2k}} - I) A_k^{-1} D_{k1} \cos(\theta(n)) \right. \\ &+ \left. (e^{A_k t_{2k}} - I) A_k^{-1} D_{k2} \sin(\theta(n)) \right) v_C(n) \\ &= \Phi_{k3} \vec{i}_{L_k}^{dq}(m) + \Gamma_{k3} \vec{V}^{dq} + \Omega_{k3} v_C(n). \end{aligned} \tag{29}$$

Using (20), (28), and (29) and knowing that

$$\begin{aligned} t_{3k} &= 2t_{0k}, \quad t_{5k} = t_{1k}, \quad t_{4k} = t_{2k}, \quad t_{7k} = t_{0k} \\ \Omega_{k_1} &= \Omega_{k_4} = \Omega_{k_7} = 0 \\ \Omega_{k_2} &= \Omega_{k_6}, \quad \Omega_{k_3} = \Omega_{k_5} \end{aligned} \tag{30}$$

we obtain the map

$$\begin{aligned} \vec{i}_{L_k}^{dq}(n+1) &= = \Phi_k \vec{i}_{L_k}^{dq}(n) + \Gamma_k \vec{V}^{dq} + \Omega_{ka} t_{k1}(n) v_C(n) \\ &+ \Omega_{kb} t_{k2}(n) v_C(n) \end{aligned} \tag{31}$$

where

$$\begin{aligned} \Phi_k &= e^{A_k T} \\ \Gamma_k &= (e^{A_k T} - I) A_k^{-1} B_k \\ \Omega_{ka} &= 2C_{k1} \cos(\theta(n)) + 2C_{k2} \sin(\theta(n)) \\ \Omega_{kb} &= 2D_{k1} \cos(\theta(n)) + 2D_{k2} \sin(\theta(n)). \end{aligned} \tag{32}$$

Using

$$\begin{aligned} t_{kd} &= \frac{1}{2} \left(\cos(\theta) + \sqrt{(3)} \sin(\theta) \right) 2t_{2k} \\ &+ \cos(\theta) 2t_{1k} \\ t_{kq} &= \frac{1}{2} \left(\sqrt{(3)} \cos(\theta) - \sin(\theta) \right) 2t_{2k} \\ &- \sin(\theta) 2t_{1k} \end{aligned} \tag{33}$$

we convert (31) to the following form:

$$\begin{aligned} \vec{i}_{L_k}^{dq}(n+1) &= F_k \left(\vec{i}_{L_k}^{dq}(n), \vec{V}^{dq}(n), \vec{t}_k^{dq}(n) \right) \\ &= \Phi_k \vec{i}_{L_k}^{dq}(n) + \Gamma_k \vec{V}^{dq} + \Omega_k \vec{t}_k^{dq}(n) \end{aligned} \tag{34}$$

where Ω_k is a diagonal matrix. Using the procedure described above, we obtain maps similar to (34) for Sectors II-VI. Now that we have obtained the discrete form of $\vec{i}_{L_k}^{dq}$, we define the following sliding surfaces to control the currents on the dq axes

$$\vec{\sigma}_k^{dq}(n) = \vec{i}^{*dq}_{L_k}(n) - \vec{i}_{L_k}^{dq}(n), \quad \vec{\sigma}_k^{dq} = [\sigma_{kd}\ \sigma_{kq}]^T. \tag{35}$$

The stability of the sliding surfaces $\vec{\sigma}_k^{dq}(n)$ is determined using the discrete Lyapunov function

$$V\left(\sigma_{kd}(n),\sigma_{kq}(n)\right)=\frac{1}{2}\vec{\sigma}_k^{dq}(n)^T\vec{\sigma}_k^{dq}(n). \tag{36}$$

For stability [31]–[34]

$$\begin{aligned}&V_{k+1}\left(\sigma_{kd}(n+1),\sigma_{kq}(n+1)\right)V_k\left(\sigma_{kd}(n),\sigma_{kq}(n)\right)\le 0\\&\Rightarrow \sigma_{kd}(n)\left(\sigma_{kd}(n+1)-\sigma_{kd}(n)\right)+\sigma_{kq}(n)\\&\cdot\left(\sigma_{kq}(n+1)-\sigma_{kq}(n)\right)\le 0.\end{aligned} \tag{37}$$

Map (34) shows that the sliding surfaces $\sigma_{kd}(n)$ and $\sigma_{kq}(n)$ have independent control, and hence the stability condition (37) is simplified to

$$\vec{\sigma}_k^{dq}(n)^T\left(\vec{\sigma}_k^{dq}(n+1)-\vec{\sigma}_k^{dq}(n)\right)\le 0. \tag{38}$$

Condition (38) is satisfied if we chose

$$\begin{aligned}&\vec{\sigma}_k^{dq}(n+1)-\vec{\sigma}_k^{dq}(n)\\&\quad=\left(-\lambda_{kd}\mathrm{sgn}\left(\sigma_{kd}(n)\right)-\lambda_{kq}\mathrm{sgn}\left(\sigma_{kq}(n)\right)\right)^T\end{aligned} \tag{39}$$

and determine $\vec{t}_k^{dq}(n)$ based on (39). In (39), λ_{kd} and λ_{kq} are scalar parameters that determine how fast the closed-loop system reaches the quasisliding surface. Substituting (35) into (39), we obtain

$$\begin{aligned}\vec{\sigma}_k^{dq}(n+1)-\vec{\sigma}_k^{dq}(n)&=\left(\vec{i}^{*dq}_{L_k}(n+1)-\vec{i}^{dq}_{L_k}(n+1)\right)\\&\quad-\vec{\sigma}_k^{dq}(n)\\&=\left(\vec{i}^{*dq}_{L_k}(n+1)-\Phi_k\vec{i}^{dq}_{L_k}(n)\right.\\&\quad\left.-\Gamma_k\vec{V}^{dq}-\Omega_k\vec{t}_k^{dq}(n)\right)-\vec{\sigma}_k^{dq}(n)\\&=\left[-\lambda_{kd}\mathrm{sgn}\left(\sigma_{kd}(n)\right)\right.\\&\quad\left.-\lambda_{kq}\mathrm{sgn}\left(\sigma_{kq}(n)\right)\right]^T\end{aligned} \tag{40}$$

and then determine $\vec{t}_k^{dq}(n)$. We then use (33) to obtain t_{1k}, t_{2k}, and $t_{0k}(=(1/2)((T/2)-t_{1k}-t_{2k}))$ from $\vec{t}_k^{dq}(n)$.

While deriving the duration of the zero vectors, we did not distinguish between the vectors U_7 and U_0. However, to control the zero-axis current, such a distinction is necessary. Let us rewrite the total duration of the zero vectors in a given switching cycle as

$$4t_{0k}=(1-\beta_k)4t_{0k}+\beta_k(4t_{0k}). \tag{41}$$

It has been shown in [26] that for the PTBC, if $\beta_2=0.5$, then by assigning $(1-\beta_1)4t_{01}$ to U_0 and $\beta_1(4t_{01})$ to U_7, one can minimize the effect of the zero-axis current. The parameter β_1 is the output of a feedback loop of M1 that regulates the zero-axis current to zero [26]. If, however, assigning $\beta_2=0.5$ is not possible (for reasons of flexibility), then one can obtain the zero vectors as a combination of the active vectors. For example, one can synthesize a reference vector $\vec{v}_r$ (for M1) in Sector I as

$$\begin{aligned}\vec{v}_r&=\frac{v_C}{2T}(t_{01}U_0+t_{11}U_1+t_{21}U_2+2t_{01}U_7+t_{21}U_2+t_{11}U_1\\&\quad+t_{01}U_0)\\&=\frac{v_C}{2T}\left(\frac{1}{2}t_{01}(U_4+U_1)+t_{11}U_1+t_{21}U_2+t_{01}(U_2+U_5)\right.\\&\quad\left.+t_{21}U_2+t_{11}U_1+\frac{1}{2}t_{01}(U_1+U_4)\right).\end{aligned} \tag{42}$$

TABLE I
NOMINAL PARAMETERS OF THE PTBC

Parameter	Nominal Value
$V_{ab}=V_{bc}=V_{ca}=V_n$	208 V (rms)
v_C (regulated)	400 V
Switching frequency $(=\frac{1}{T})$	32kHz
$L_1=L_2=L_n$	500 μH
$r_{L_1}=r_{L_2}=r_{L_n}$	0.5 Ω
C	1200 μF
R	4 Ω
Power rating of M1 and M2	20 kVA

Although this scheme increases the flexibility of operation, it can not completely control the circulation of the zero-axis current. Hence, the zero-axis disturbance can be controlled by the size of the line inductor and the switching frequency of the converter.

V. RESULTS

We present simulation results obtained by closing the PTBC using three different controllers. The first one is a conventional dq-axes controller, which is described in [10], [11]. The second controller (CS_{Ye}) is due to Ye *et al.* [26]. The third $(\mathrm{CS}_{discrete})$ is our proposed discrete nonlinear controller. The values of the nominal parameters for the PTBC are listed in Table I. The load is chosen to be resistive in nature and has a magnitude of R. However, the proposed control scheme $\mathrm{CS}_{discrete}$ can be applied to systems that involve other types of loads because they are independent of the load type.

For all the three controllers and as shown in Fig. 4, the outer voltage loop, which regulates the bus voltage at 400 volts, has been chosen to have a slower dynamic response as compared to that of the inner current loops to ensure stability of the overall system [35]. The choice of the parameters for the voltage loop are based on the results of [15]. The output of the voltage controller serves as the reference for the d-axis current. The reference for the q-axis current is set to zero for unity power-factor operation. The o-axis current reference for CS_{Ye} and $\mathrm{CS}_{discrete}$ is set to zero to minimize circulating current between the two power modules of the PTBC. The choice of the controller parameters for the current loop of the conventional dq-axes controller and CS_{Ye} are described in [10], [11] and [26], respectively. Design of the current controller for $\mathrm{CS}_{discrete}$ is outlined in Section IV-B. To close the current loops in dq or dqo frames, the stationary (abc) frame currents in (2) are transformed to synchronous (dqo) frame using the transformation $T(\theta)$ described in Appendix II. For all the three controllers, the output of the

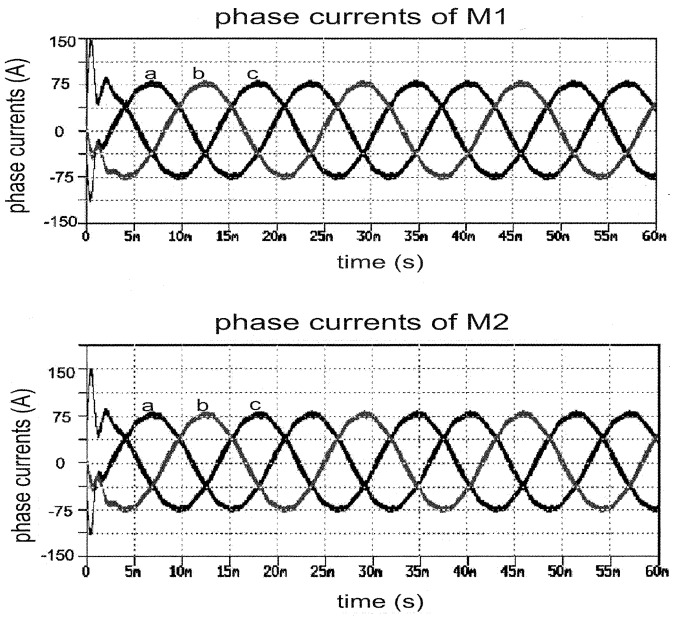

Fig. 6. Results obtained using a conventional dq controller for two similar modules (i.e., the values of the parameters of M1 and M2 are identical). Clearly, the phase currents are balanced.

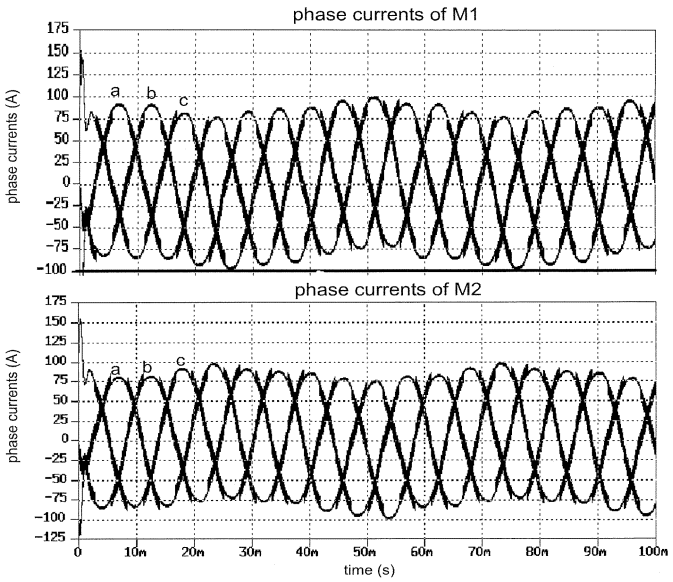

Fig. 7. Phase currents of M1 and M2 using a conventional controller when the parameters of the modules are the same, except L_1 is 95% of L_2. The result shows the limitation of a conventional dq controller in ensuring even-load distribution when the two modules have parametric variations.

current-loop controllers are used to derive the reference voltage vector (shown in Fig. 3), which is then used to obtain the durations for which the active and zero space vectors are turned on. The procedure to obtain these time durations for conventional dq-axes controller and CS_{Ye} are described in [10], [11] and [26], respectively. For the $\mathrm{CS}_{discrete}$, durations for the active and zero states are obtained using (30), (33), (40), and (41).

Using a conventional dq controller [7], [8], [11], [15] operating with the bus-clamped SVM [8], [36], we show in Fig. 6 the steady-state responses obtained for the case in which the parameters of M1 and M2 are equal to the nominal values and the switching instants of the two modules are half a switching cycle apart (interleaved operation) [7], [8]. Clearly, the phase currents are balanced. The two modules operate with interleaving to minimize the ripple in the output voltage. We chose the bus-clamped SVM scheme [8] to reduce the switching loss of the PTBC and increase its efficiency. In addition, for power-factor-correction (PFC) applications, the bus-clamped SVM scheme is the most favorable because, in a given sector, the phase carrying the highest current is connected to the bus permanently [36], [38].

In practice, it is impossible to manufacture two identical modules. In fact, it is not uncommon to have variations in the circuit parameters of the order of 5%. To simulate one such scenario, we reduce L_1 by 5% from its nominal value, but keep the values of all of the other parameters of M1 equal to their nominal values. Moreover, we keep the values of the parameters of M2 equal to their nominal values. Furthermore, the two modules operate with interleaving and use the same SVM scheme [8]. In Fig. 7, we show that, even though there is only a minor difference in one of the parameters of the two modules, the phase currents in each module are no more balanced.

In Fig. 8, we show projections of the averaged values of the unbalanced phase currents (of M1) in the dqo frame onto the $\alpha\beta$o axes. It show that, while the d and q components on the $\alpha\beta$

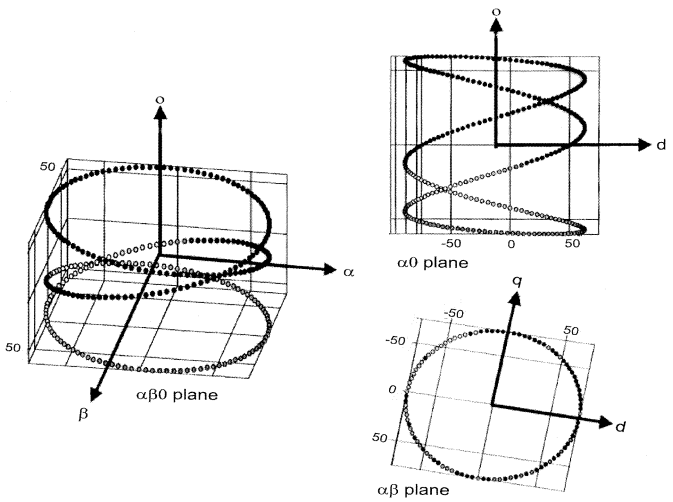

Fig. 8. Three-dimensional view of the unbalanced phase currents of M1 in the $\alpha\beta o$ frame. It shows that a conventional dq controller can not see the zero-sequence current because it lies on a perpendicular axis.

plane still rotate in a circle, the zero-axis component oscillates up and down. The flow of the zero-sequence current causes a strong oscillation in the phase currents of the two modules. Consequently, the load sharing between M1 and M2 is poor. Thus, the performance of a conventional dq control scheme is not satisfactory even under small parametric variations.

In Fig. 9, we demonstrate the steady-state performance of the PTBC operating with CS_{Ye} [26]. The values of the parameters are the same as those used to obtain Figs. 9 and 10. We see that, by controlling the zero-sequence current in addition to the dq currents, the steady-state performance becomes satisfactory. Although the zero-sequence current is not eliminated, its overall effect is minimized.

Next, we explore the dynamic performances of the PTBC using our proposed control scheme $\mathrm{CS}_{discrete}$ and CS_{Ye} under

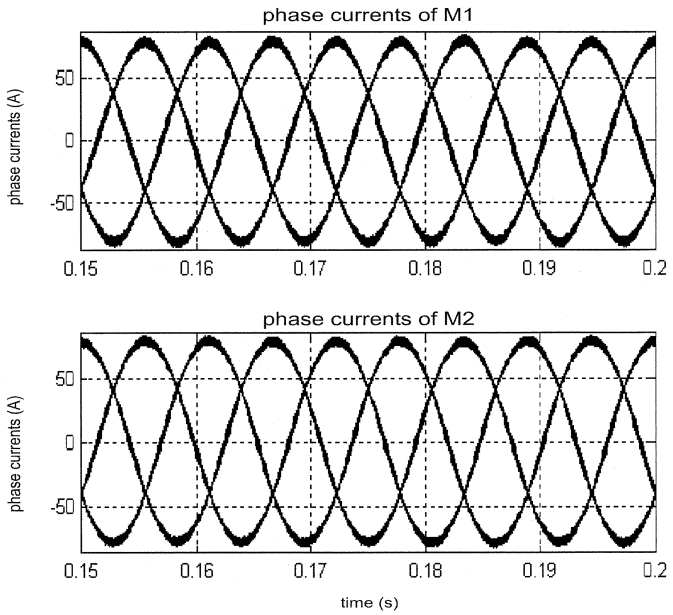

Fig. 9. Phase currents of M1 and M2 obtained using CS_{Ye} when the parameters of the modules are the same, except L_1 is 95% of L_2. By adding a zero-sequence controller, the effect of the overall unbalance as seen in Fig. 8 has been minimized.

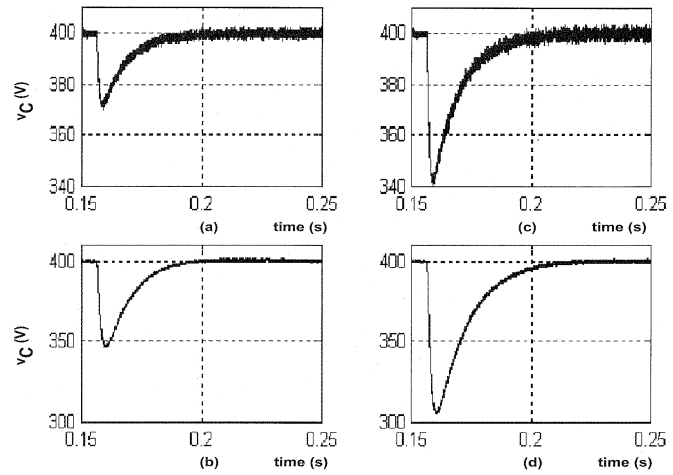

Fig. 10. Change in the bus voltage obtained using $\mathrm{CS}_{discrete}$ (a, c) and CS_{Ye} (b, d) for case one (figures on the left) and case two (figures on the right). For either case, the drop in the bus voltage is larger when using CS_{Ye}, even though it is implemented for a smaller variation (5%) L_1 as compared to the proposed control scheme (15%).

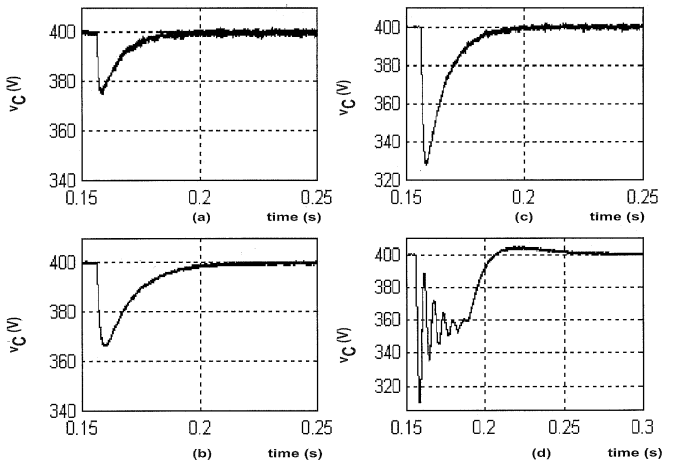

Fig. 11. Drop in the bus voltage obtained using $\mathrm{CS}_{discrete}$ (a, c) and CS_{Ye} (b, d) for cases three (figures on the left) and four (figures on the right). For both cases, the drop in the bus voltage is larger when using CS_{Ye}, even though it is implemented for a smaller variation (5%) L_1 as compared to the proposed control scheme (15%).

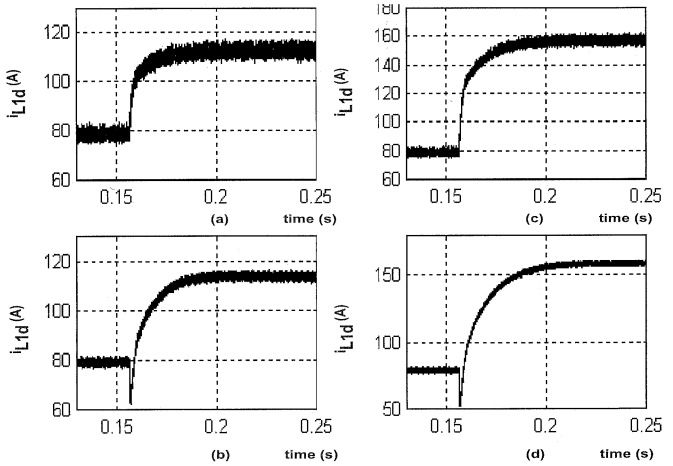

Fig. 12. Change in the active current of M1 obtained using $\mathrm{CS}_{discrete}$ (a, c) and CS_{Ye} (b, d) for case one (figures on the left) and case two (figures on the right). Although $\mathrm{CS}_{discrete}$ operates with a larger variation in L_1, its performance is good. Using CS_{Ye}, there is more than a 30% undershoot in i_{L1d} immediately after the disturbances.

further variations in the parameters of the two modules. The switching frequencies of M1 and M2 are set at 16 kHz and 32 kHz, respectively, to replicate the conditions in [26]. In real life, the two modules will be physically apart, and hence synchronization of the clocks is expensive and not reliable [8], [9]. Hence, to increase the redundancy of operation, we switch M1 and M2 asynchronously. To test the robustness of CS_{Ye} under parametric variation, we reduce L_1 by 5% from its nominal value. We test the robustness of $\mathrm{CS}_{discrete}$ by reducing L_1 by 5% and 15%, an even larger variation in its nominal value. The larger variation in L_1, which makes paralleling M1 and M2 even more difficult [8], is chosen to test the robustness of the nonlinear controller under extreme conditions. For both the control schemes, the values of all of the other parameters are kept equal to their nominal values. We found that, using the proposed control scheme, the performance for smaller variations in L_1 is excellent. Due to the limitation in space and to avoid duplication, we only demonstrate the performance of $\mathrm{CS}_{discrete}$ for the larger (15%) variation in L_1. If the closed-loop system performs satisfactorily for large parametric variations, it will certainly perform satisfactorily for small parametric variations.

Having set the operating parameters, we determine the response of the PTBC (using $\mathrm{CS}_{discrete}$ and CS_{Ye}) under small- and large-signal feedforward and feedback disturbances: four cases are considered. For both cases, we investigate the performance of the PTBC by determining the drop in its bus voltage, the change in its reactive and active currents, the power factor, and the current sharing between the modules.

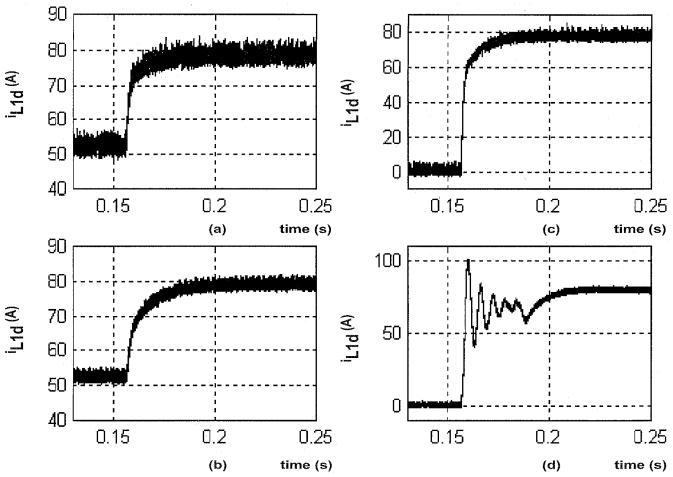

Fig. 13. Change in the active current of M1 using $\mathrm{CS}_{discrete}$ (a, c) and CS_{Ye} (b, d) for case three (figures on the left) and case four (figures on the right). The performance of the proposed control scheme is satisfactory, even though it operates with a larger variation in L_1. The performance of CS_{Ye}, for case four, is not satisfactory. Besides, CS_{Ye} has a slower recovery time for case three.

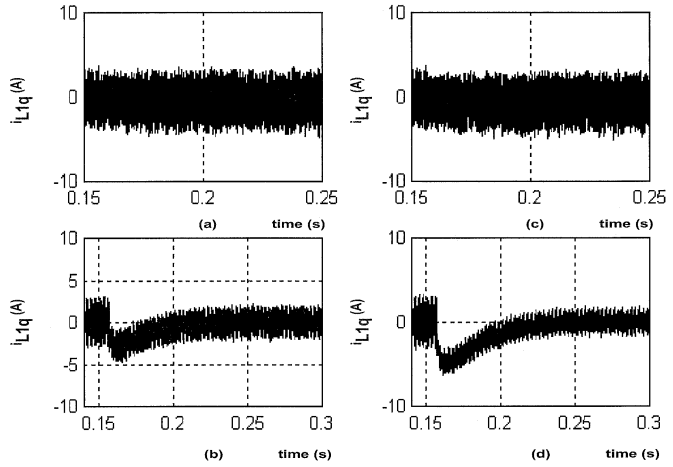

Fig. 14. Change in the reactive current of M1 obtained using $\mathrm{CS}_{discrete}$ (a, c) and CS_{Ye} (b, d) for case one (figures on the left) and case two (figures on the right). The performance of the proposed control scheme is good, even though it operates with a larger variation in L_1. However, CS_{Ye} fails to maintain the average of i_{L1q} at zero immediately after the disturbance. This weakens the decoupling between i_{L1d} and i_{L1q} and hence the dynamic response of the PTBC suffers.

For case one, we subject the PTBC, operating in steady-state, to a sudden change in the input voltage. Initially, the input voltage is set equal to its nominal value, and after the transient, it is assumed to decrease to 30% of its nominal value. We begin by investigating the drop in the bus voltage. The results are shown in Fig. 10(a) and (b). We find out that the dip in the bus voltage is maximum when the PTBC is operated using CS_{Ye}. In addition, for this control scheme, the recovery time for the bus voltage is longer. The ripple in the bus voltage obtained using $\mathrm{CS}_{discrete}$ is marginally higher than that obtained with CS_{Ye} because the former operates with $L_1 = 0.85L_n$ and $L_2 = L_n$ compared to $L_1 = 0.95L_n$ and $L_2 = L_n$ for CS_{Ye}. Thus, even with a larger parametric variation, the performance of the proposed control scheme are better than that obtained using the control scheme proposed by Ye *et al.* [26].

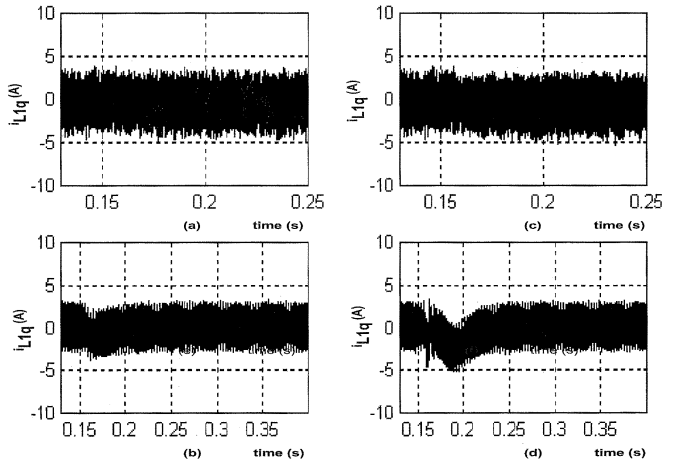

Fig. 15. Change in the reactive current of M1 obtained using $\mathrm{CS}_{discrete}$ (a, c) and CS_{Ye} (b, d) for case three (figures on the left) and case four (figures on the right). The performance of the proposed control scheme is good, even though it operates with a larger variation in L_1. For case four, CS_{Ye} fails to maintain the average of i_{L1q} at zero immediately after the disturbance. This weakens the decoupling between i_{L1d} and i_{L1q} and hence the dynamic response of the PTBC suffers.

Case two is similar to case one, except that the drop in the input voltage is larger, 50% of its nominal value. We plot the changes in the bus voltage obtained with all of the control schemes. Fig. 10(c) and (d) show that, with a larger feedforward disturbance, the dip in the bus voltage is larger and the recovery time is longer for all of the control schemes. However, the drop in the bus voltage and the recovery time obtained with CS_{Ye}, are, respectively, larger and longer than those obtained with $\mathrm{CS}_{discrete}$ even though CS_{Ye} is implemented for a smaller variation in L_1.

For case three, we subject the PTBC, operating in steady-state, to a sudden change in the load resistance from 6 Ω to 4 Ω (nominal value). Fig. 11(a) and (b) show that the change in the bus voltage obtained using $\mathrm{CS}_{discrete}$ is smaller than that obtained with CS_{Ye}. Moreover, the recovery time obtained using CS_{Ye} is longer.

Finally, for case four, we subject the PTBC to an even larger change in the load resistance from 400 Ω (almost no load) to full load (4 Ω). The results are shown in Fig. 11(b) and (d). We see that the regulation of the bus voltage, immediately after the disturbance, is the poorest when the PTBC is controlled using CS_{Ye}. Moreover, the recovery time of the bus voltage obtained with CS_{Ye} is the longest.

Next, we investigate the performances of the inner (dq) current loops for all cases under feedforward and feedback disturbances. The higher the disturbance rejection capability of these loops is, the lesser the impact of these disturbances on the bus voltage is. Using the same procedure as described above, we first investigate the response of the d-axis (active) current using both the control schemes. Fig. 12(a) and (b) show the response of the active current of M1 (i.e., i_{L1d}) for case one. Later on, we will show the currents of both modules. We see from the figures that, using the proposed control scheme, the PTBC does not have any undershoot after the feedforward disturbance. However, the parallel converter shows a significant drop in the i_{L1d} when using CS_{Ye}. Because of this undershoot, the drops in the

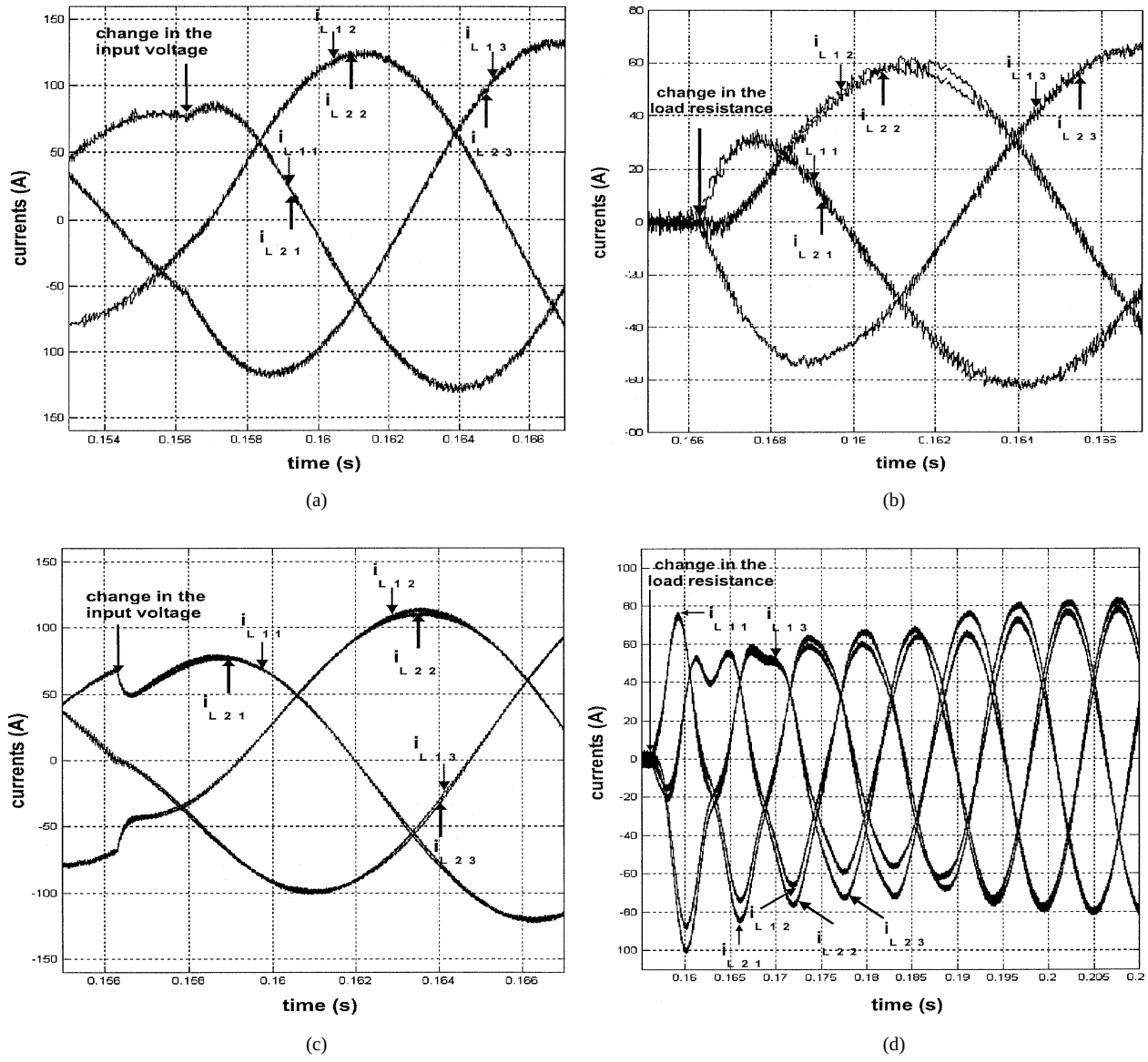

Fig. 16. Distribution of the line currents between M1 and M2 obtained using $\mathrm{CS}_{discrete}$ (a, b) and CS_{Ye} (c, d) when the PTBC is subjected to a large disturbance in the input voltage (case two) and the load (case four). The proposed control scheme and CS_{Ye} operate with $L_1 = 85\% L_n$ and $L_1 = 95\% L_n$, respectively.

bus voltage obtained using CS_{Ye}, as shown in Figs. 10 and 11, are higher.

For case two, the i_{L1d} obtained using $\mathrm{CS}_{discrete}$ and CS_{Ye} are shown in Fig. 12(c) and (d), respectively. The overall responses are similar to those obtained in case one. However, the recovery times using all schemes increase. Moreover, when the PTBC operates with CS_{Ye}, there is a further increase in the undershoot of i_{L1d}. The ripple in the i_{L1d} using $\mathrm{CS}_{discrete}$ is higher because they operate with $L_1 = 0.85L_n$ and $L_2 = L_n$ as compared to $L_1 = 0.95L_n$ and $L_2 = L_n$ for CS_{Ye}. The responses of i_{L1d} for cases three and four, shown in Fig. 13(a)–(d), are self explanatory and similar to those obtained for cases one and two. We see that the performance of the PTBC operating with CS_{Ye} suffers considerably for large load disturbances. No such shortcoming was observed for the proposed control scheme. Therefore, even with larger parametric variations, the disturbance rejection capabilities of the proposed control scheme is better than that of CS_{Ye}.

We then investigate the response of the q-axis (reactive) current of the PTBC for both the cases. The results are shown in Figs. 14 and 15 for M1. We see that, under steady-state conditions, the average of i_{L1q} obtained using all control schemes is about zero. As such, the input power factor of the PTBC is close to unity. However, for either a large disturbance in the load or the input voltage, CS_{Ye} is unable to maintain the average of i_{L1q} at zero immediately after the disturbance. As such, the perfect decoupling between i_{L1d} and i_{L1q} is lost and the rate of transfer of power from the input to the load deteriorates [15]. For $\mathrm{CS}_{discrete}$, i_{L1q} does not have any undershoot after the disturbances. Therefore, it follows from Figs. 12–15 that, unlike CS_{Ye}, the proposed control scheme maintains decoupling even under severe feedforward or feedback disturbances and hence is more robust [15].

Next, we investigate the sharing of the line currents between M1 and M2, when the PTBC is subjected to a large disturbance in either the voltage (case two) or the load (case four). Fig. 16(a)

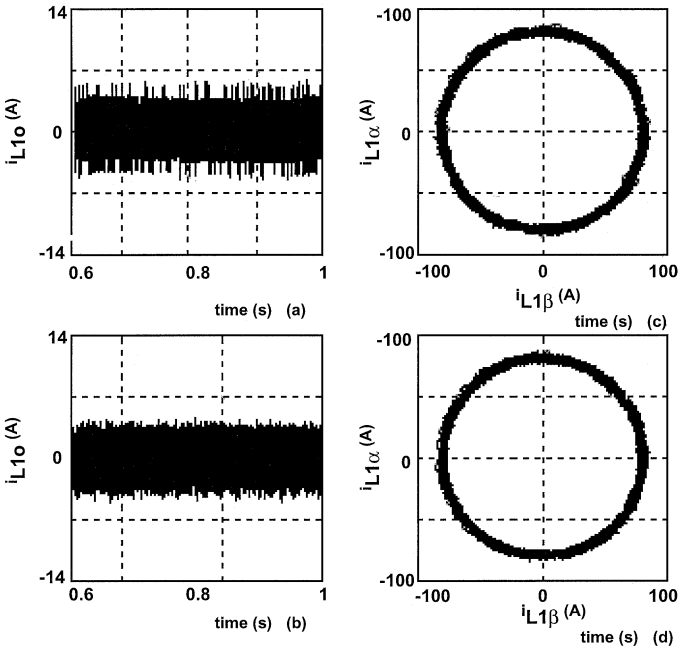

Fig. 17. Steady-state currents on the zero axis and the $\alpha\beta$ axes for M1 obtained using $\mathrm{CS}_{discrete}$ (a, c) and CS_{Ye} (b, d). Both the cases have the same parametric variations. As such, the harmonic distortion and the zero-sequence current of CS_3 and CS_{Ye} are close.

and (c) show the performance of the PTBC for case two using $\mathrm{CS}_{discrete}$ and CS_{Ye}. For this case, we see that the best transient response is achieved using $\mathrm{CS}_{discrete}$. The recovery time of the PTBC obtained with CS_{Ye} is the largest. Moreover, immediately after the change in the voltage, there is an undershoot and an overshoot in two of the phase currents, which are not evident in the responses obtained with the proposed control scheme.

Fig. 16(b) and (d) show the performance of the PTBC for case four using $\mathrm{CS}_{discrete}$ and CS_{Ye}, respectively. The response of the PTBC obtained with CS_{Ye} is significantly inferior to that of the proposed control scheme, both in terms of the response time and current sharing. Thus, even with a larger parametric variation, the performance of $\mathrm{CS}_{discrete}$ is better than that of CS_{Ye}.

Finally, we show the impact of the control schemes $\mathrm{CS}_{discrete}$ and CS_{Ye} on the steady-state ripples of the phase currents (in the $\alpha\beta$ frame) and on the zero-axis current that circulates between the two modules in Fig. 17(a)–(d). For all of these plots, we chose $L_1 = 0.85L_n$ and $L_2 = L_n$. All other parameters are kept the same as before. We note that, the smaller the magnitude of the zero-axis current is, the more effective the load sharing between the two modules is. The steady-state ripple and the zero-axis current obtained using both schemes are practically the same.

VI. Conclusion

We compare the performances of the proposed controller with a conventional dq-axes controller [7] and another controller, which was recently proposed by Ye *et al.* [26]. We find that the conventional dq-axes controller fails to stabilize the PTBC even for slight parametric variations of the two modules. This is because the conventional dq-axes controller does not control the current on the zero axis, which is perpendicular to the dq-axes.

The controller proposed by Ye *et al.* [26] performs better than the conventional dq-axes controller. However, its transient response, when the input voltage and the load drop to about 30% of their nominal values, is inferior to the proposed control scheme. For even larger disturbances, the dynamic performance of the controller proposed by Ye *et al.* [26] suffers considerably. We find that, if the input voltages drops to 50% of its rated value then, the dips in the bus voltage and the active current are about 25% and 35%, respectively, of their nominal values. For the same disturbance, using the proposed control scheme, the drop in the bus voltage is about 15%. The active current does not show any undershoot. When the PTBC is subjected to a change in the load from almost no load to full load, the control scheme proposed by Ye *et al.* [26] barely stabilizes the system. The undershoot and the overshoot in the bus voltage and the active currents are about 25% and 28%, respectively. Furthermore, the recovery time is considerably longer than obtained with the proposed control scheme. The drop in the bus voltage, using the proposed control scheme, is about 16% of its nominal value. Besides, the active current does not show any undershoot.

The effectiveness of the controller proposed by Ye *et al.* [26] deteriorates under saturated conditions because the zero vectors cannot be applied [26]. Under saturated conditions, the proposed control shares the same limitation as that proposed by Ye *et al.* [26]. However, unlike the latter, the proposed controller guarantees global stability within the boundary layer [40]. That is why its transient performance is better.

The proposed discrete controller combines space-vector modulation with variable-structure controller within the boundary layer. This ensures that under steady-state condition, the switching frequency of the parallel three-phase boost converter is constant.

The operation of the proposed controller does not require any communication between the modules. Therefore, the proposed controller has high redundancy and can be extended to a parallel three-phase converter operating with more than two modules. Furthermore, using the new controller the modules operate asynchronously with different switching frequencies in the presence of variations in circuit parameters.

Appendix I

$$P_{11} = -\frac{r_{L_1}}{3L_1(L_1+L_2)} \times \begin{bmatrix} 3L_1+2L_2 & -L_2 & -L_2 \\ -L_2 & 3L_1+2L_2 & -L_2 \\ -L_2 & -L_2 & 3L_1+2L_2 \end{bmatrix}$$

$$P_{12} = -\frac{r_{L_2}}{3(L_1+L_2)} \begin{bmatrix} 1 & 1 & 1 \\ 1 & 1 & 1 \\ 1 & 1 & 1 \end{bmatrix}$$

$$P_{13} = \frac{1}{3L_1} \begin{bmatrix} 2 & -1 & -1 \\ -1 & 2 & -1 \\ -1 & -1 & 2 \end{bmatrix}$$

$$P_{14} = -\frac{1}{6L_1(L_1+L_2)}$$

$$T(\theta)=\frac{2}{3}\begin{bmatrix}\cos(\theta) & \cos\left(\theta-\frac{2\pi}{3}\right) & \cos\left(\theta-\frac{4\pi}{3}\right)\\ -\sin(\theta) & -\sin\left(\theta-\frac{2\pi}{3}\right) & -\sin\left(\theta-\frac{4\pi}{3}\right)\\ \frac{1}{\sqrt{2}} & \frac{1}{\sqrt{2}} & \frac{1}{\sqrt{2}}\end{bmatrix}$$

$$[T(\theta)]^{-1}=\begin{bmatrix}\cos(\theta) & -\sin(\theta) & \frac{1}{\sqrt{2}}\\ \frac{1}{2}\left(-\cos(\theta)+\sqrt{3}\sin(\theta)\right) & \frac{1}{2}\left(\sqrt{3}\cos(\theta)+\sin(\theta)\right) & \frac{1}{\sqrt{2}}\\ \frac{1}{2}\left(-\cos(\theta)-\sqrt{3}\sin(\theta)\right) & \frac{1}{2}\left(-\sqrt{3}\cos(\theta)+\sin(\theta)\right) & \frac{1}{\sqrt{2}}\end{bmatrix}$$

$$\frac{d}{d\theta}[T(\theta)]^{-1}=\omega\begin{bmatrix}-\sin(\theta) & -\cos(\theta) & 0\\ \frac{1}{2}\left(\sin(\theta)+\sqrt{3}\cos(\theta)\right) & \frac{1}{2}\left(-\sqrt{3}\sin(\theta)+\cos(\theta)\right) & 0\\ \frac{1}{2}\left(\sin(\theta)\sqrt{3}\cos(\theta)\right) & \frac{1}{2}\left(\sqrt{3}\sin(\theta)+\cos(\theta)\right) & 0\end{bmatrix}$$

$$\times\begin{bmatrix}3L_1+2L_2 & -L_2 & -L_2\\ -L_2 & 3L_1+2L_2 & -L_2\\ -L_2 & -L_2 & 3L_1+2L_2\end{bmatrix}$$

$$P_{15}=\frac{1}{6L_1(L_1+L_2)}\begin{bmatrix}L_1 & L_1 & L_1\\ L_1 & L_1 & L_1\\ L_1 & L_1 & L_1\end{bmatrix}$$

$$P_{21}=-\frac{r_{L_1}}{3(L_1+L_2)}\begin{bmatrix}1 & 1 & 1\\ 1 & 1 & 1\\ 1 & 1 & 1\end{bmatrix}$$

$$P_{22}=-\frac{r_{L_2}}{3L_2(L_1+L_2)}$$

$$\times\begin{bmatrix}3L_2+2L_1 & -L_1 & -L_1\\ -L_1 & 3L_2+2L_1 & -L_1\\ -L_1 & -L_1 & 3L_2+2L_1\end{bmatrix}$$

$$P_{23}=\frac{1}{3L_2}\begin{bmatrix}2 & -1 & -1\\ -1 & 2 & -1\\ -1 & -1 & 2\end{bmatrix}$$

$$P_{24}=\frac{1}{6L_2(L_1+L_2)}\begin{bmatrix}L_2 & L_2 & L_2\\ L_2 & L_2 & L_2\\ L_2 & L_2 & L_2\end{bmatrix}$$

$$P_{25}=-\frac{1}{6L_2(L_1+L_2)}$$

$$\times\begin{bmatrix}3L_2+2L_1 & -L_1 & -L_1\\ -L_1 & 3L_2+2L_1 & -L_1\\ -L_1 & -L_1 & 3L_2+2L_1\end{bmatrix}$$

APPENDIX II

(See equation at the top of the page).

REFERENCES

[1] S. Ogasawara, J. Takagaki, H. Akagi, and A. Nabae, "A novel control scheme of duplex current-controlled PWM inverters," in *Proc. IEEE Ind. Applicat. Soc.*, 1987, pp. 330–337.

[2] I. Takahashi and M. Yamane, "Multiparallel asymmetrical cycloconverter having improved power factor and waveforms," *IEEE Trans. Ind. Applicat.*, vol. 22, pp. 1007–1016, Nov./Dec. 1986.

[3] T. Kawabata and S. Higashino, "Parallel operation of voltage source inverters," *IEEE Trans. Ind. Applicat.*, vol. 24, pp. 281–287, Mar./Apr. 1988.

[4] J. W. Dixon and B. T. Ooi, "Series and parallel operation of hysterisis current-controlled PWM rectifiers," *IEEE Trans. Ind. Applicat.*, vol. 25, pp. 644–651, July/Aug. 1989.

[5] Y. Komatsuzaki, "Cross current control for parallel operating three-phase inverter," in *Proc. IEEE Power Electron. Spec. Conf.*, 1994, pp. 943–950.

[6] Z. Zhang and B. Ooi, "Multimodular current-source SPWM converters for superconducting a magnetic energy storage system," *IEEE Trans. Power Electron.*, vol. 8, pp. 250–256, May 1993.

[7] K. Xing, S. K. Mazumder, Z. Ye, D. Boroyevich, and F. C. Lee, "The circulating current in paralleled three-phase boost PFC rectifiers," in *Proc. IEEE Power Electron. Spec. Conf.*, 1999, pp. 783–789.

[8] K. Xing, F. C. Lee, D. Boroyevich, Z. Ye, and S. K. Mazumder, "Interleaved PWM with discontinuous space-vector modulation," *IEEE Trans. Power Electron.*, vol. 14, pp. 250–256, Sept. 1999.

[9] S. K. Lee, S. K. Lipo, B. J. Baliga, A. Ramamurthy, A. W. Kelley, and K. Armstrong *et al.*, "Power Electronics Building Blocks and System Integration," Tech. Rep., Office of Naval Research, Virginia Power Electronics Center, Blacksburg, VA, 1997.

[10] T. G. Habetler, "A space-vector based rectifier regulator for ac/dc/ac converters," in *Proc. Eur. Conf. Power Electron. Applicat.*, vol. 2, 1991, pp. 101–107.

[11] S. Hiti, D. Boroyevich, and C. Cuadros, "Small signal modeling and control of three-phase PWM converters," in *Proc. IEEE Ind. Applicat. Soc.*, 1994, pp. 1143–1150.

[12] S. K. Mazumder, "DSP based implementation of a PWM ac/dc/ac converter using space-vector-modulation with primary emphasis on the analysis of the practical problems involved," in *Proc. Appl. Power Electron. Conf.*, 1997, pp. 306–312.

[13] Y. Sato and T. Kataoka, "Simplified control strategy to improve ac input-current waveform of parallel connected current-type PWM rectifiers," in *Proc. Inst. Elect. Eng.*, vol. 142, 1995, pp. 246–254.

[14] K. Matsui, "A pulsewidth modulated inverter with parallel-connected transistors by using current sharing reactors," in *Proc. Ind. Applicat. Soc.*, 1985, pp. 1015–1019.

[15] S. Hiti, "Modeling and Control of Three-Phase PWM Converters," Ph.D. dissertation, Dept. Elect. Comput. Eng., Virginia Polytech. Inst. State Univ., Blacksburg, VA, 1995.

[16] A. F. Filippov, *Differential Equations With Discontinuous Righthand Sides*. Amsterdam, The Netherlands: Kluwer, 1988.

[17] V. Utkin, *Sliding Modes in Control Optimization*. New York: Springer-Verlag, 1992.

[18] N. S. Behilovic, T. Ninomiya, A. Sabanovic, and B. Perunicic, "Control of three-phase switching converters: a sliding mode approach," in *Proc. IEEE Power Electron. Spec. Conf.*, 1993, pp. 630–635.

[19] S. K. Mazumder, A. H. Nayfeh, and D. Boroyevich, "Robust control of parallel dc-dc buck converters by combining integral-variable-structure control and multiple-sliding surface control schemes," *IEEE Trans. Power Electron.*, vol. 17, pp. 428–437, May 2000.

[20] I. Nagy, "Novel adaptive tolerance band based PWM for field-oriented control of induction machines," *IEEE Trans. Ind. Electron.*, vol. 41, pp. 406–417, Aug. 1994.

[21] V. D. Broeck, H. C. Skudelny, and G. Stanke, "Analysis and realization of a pulse width modulator based on voltage space vectors," *IEEE Trans. Ind. Electron.*, vol. 1, pp. 142–150, 1988.

[22] S. Ogasawara, H. Akagi, and A. Nabae, "A novel PWM scheme of voltage source inverters based on space vector theory," in *Proc. Eur. Power Electron. Conf.*, 1989, pp. 1197–1202.

[23] J. H. Holtz, W. Lotzkat, and A. M. Khambadkone, "On continuous control of PWM inverters in the overmodulation range including the six step mode," *IEEE Trans. Power Electron.*, vol. 8, pp. 546–553, July 1993.

[24] V. R. Stefanovic and S. N. Vukosavic, "Space vector PWM voltage control with optimized switching strategy," *IEEE Trans. Ind. Applicat.*, pp. 1025–1035, 1994.

[25] T. G. Habetler, F. Perfumo, M. Pastorelli, and L. M. Tolbert, "Direct torque control of induction machines using space vector modulation," *IEEE Trans. Ind. Applicat.*, vol. 28, pp. 1045–1053, Sept./Oct. 1992.
[26] Z. Ye, D. Boroyevich, J. Y. Choi, and F. C. Lee, "Control of circulating current in parallel three-phase boost converters," in *Proc. Appl. Power Electron. Conf.*, 2000.
[27] S. K. Mazumder, M. Alfayyoummi, A. H. Nayfeh, and D. Boroyevich, "A theoretical and experimental investigation of the nonlinear dynamics of dc-dc converters," in *Proc. IEEE Power Electron. Spec. Conf.*, 2000, pp. 729–734.
[28] M. Alfayyoumi, A. H. Nayfeh, and D. Boroyevich, "Modeling and analysis of switching-mode dc-dc regulators," *Int. J. Bifurcation Chaos*, 2000.
[29] S. K. Mazumder, A. H. Nayfeh, and D. Boroyevich, "A theoretical and experimental investigation of the fast- and slow-scale instabilities of a dc-dc converter," *IEEE Trans. Power Electron.*, vol. 16, Mar. 2001.
[30] ——, "Nonlinear analysis of parallel dc-dc converters," *JVC: Special Issue Nonlinear Dynam. Control*, 2002.
[31] D. Milosavljevic, "General conditions for the existence of a quasisliding mode on the switching hyperplane in discrete variable structure systems," *Automat. Remote Control*, vol. 46, pp. 307–314, 1985.
[32] S. Z. Sarpturk, Y. Istefanopulos, and O. Kaynak, "On the stability of discrete-time sliding mode control systems," *IEEE Trans. Automat. Control*, vol. 32, pp. 930–932, Oct. 1987.
[33] U. Kotta, "On the stability of discrete-time sliding mode control systems," *IEEE Trans. Automat. Control*, vol. 34, pp. 1021–1022, Sept. 1989.
[34] K. Furuta, "Sliding mode control of a discrete system," *Syst. Control Lett.*, vol. 14, pp. 145–152, 1990.
[35] S. K. Mazumder, A. H. Nayfeh, and D. Boroyevich, "A novel approach to the stability analysis of boost power-factor-correction circuits," in *Proc. IEEE Power Electron. Spec. Conf.*, 2001, pp. 1719–1724.
[36] V. H. Prasad, D. Boroyevich, and S. Dubovsky, "Comparison of high frequency PWM algorithms for voltage source inverters," in *Proc. Virginia Power Electron. Center Sem.*, 1996, pp. 115–122.
[37] P. Korondi, L. Nagi, and G. Nemeth, "Control of a three phase ups inverter with unbalanced and nonlinear load," in *Proc. Eur. Conf. Power Electron. Firenze*, vol. 3, 1991, pp. 180–184.
[38] S. K. Mazumder, "Complete mathematical analysis of ripple current as a function of the modulation index for direct indirect and bus clamped space vector modulation techniques," in *Proc. IEEE Elect. Machines Drives Conf.*, 1997, pp. TC2/10.1–TC2/10.3.
[39] J. Holtz, "Pulsewidth modulation—a survey," *IEEE Trans. Ind. Electron.*, vol. 39, Oct. 1992.
[40] S. K. Mazumder, "Nonlinear analysis and control of standalone, parallel dc-dc, and parallel multi-phase PWM converters," Ph.D. dissertation, Dept. Elect. Comput. Eng., Virginia Polytech. Instit. State Univ., Blacksburg, VA, 2001.

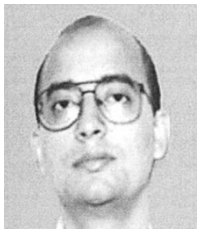

Sudip K. Mazumder (M'01) received the M.S. degree in electrical power engineering from the Rensselaer Polytechnic Institute (RPI), Troy, NY, in 1993 and the Ph.D. degree in electrical and computer engineering from the Virginia Polytechnic Institute and State University (VPI&SU), Blacksburg, VA, in 2001.

He is currently an Assistant Professor at the Power Electronics Research Center (PERC), Department of Electrical and Computer Engineering, University of Illionoic, Chicago. He has over 10 years of experience and has held R&D and design positions in leading industrial organizations. he has published over 35 refereed and invited journal and conference papers and is a Reviewer for six international journals. His areas of expertise and interest include interactive power/power-electronic networks (IPNs), renewable/alternative energy systems and distributed generation, optical switching in power electronics, wireless motion sensing and wide-area power management, advanced control and DSP/RISC and ASIC-based embedded controllers for power supplies/systems and motor drives, power quality and voltage sags, soft-switching and hard-switching topologies and techniques in power converters, and packaging.

Dr. Mazumder received the DOE SECA Award in 2002, the NSF CAREER Award in 2003, and the Prize Paper Award from the IEEE TRANSACTIONS ON POWER ELECTRONICS and the IEEE Power Electronics Society, in 2002, and the Solid-State Energy Conversion Alliance (SECA) Award from the Department of Energy in 2002. He is listed in *Who's Who in Engineering Education*. He is an Associate Editor of the IEEE TRANSACTIONS ON INDUSTRIAL ELECTRONICS and the IEEE POWER ELECTRONICS LETTERS.